Fe Vibrational Spectroscopy of Myoglobin and Cytochrome *f*

Kristl L. Adams,[⊥] Stanislav Tsoi,[⊥] Jiusheng Yan,[†] Stephen M. Durbin,*[,⊥] Anant K. Ramdas,[⊥] William A. Cramer,[†] Wolfgang Sturhahn,[‡] E. Ercan Alp,[‡] and Charles Schulz[§]

Department of Physics and Department of Biological Sciences, Purdue University, West Lafayette, Indiana 47907, Advanced Photon Source, Argonne National Laboratory, Argonne, Illinois 60439, and Department of Physics, Knox College, Galesburg, Illinois 61401

Received: June 24, 2005; In Final Form: October 25, 2005

The Fe vibrational density of states (VDOS) has been determined for the heme proteins deoxymyoglobin, metmyoglobin, and cytochrome *f* in the oxidized and reduced states, using nuclear resonance vibrational spectroscopy (NRVS). For cytochrome *f* in particular, the NRVS spectrum is compared with multiwavelength resonance Raman spectra to identify those Raman modes with significant Fe displacement. Modes not seen by Raman due to optical selection rules appear in the NRVS spectrum. The mean Fe force constant extracted from the VDOS illustrates how Fe dynamics varies among these four monoheme proteins, and is correlated with oxidation and spin state trends seen in model heme compounds. The protein's contribution to Fe motion is dominant at low frequencies, where coupling to the backbone tightly constrains Fe displacements in cytochrome *f*, in contrast to enhanced heme flexibility in myoglobin.

I. Introduction

In this study we utilize a new window into heme protein dynamics, nuclear resonance vibrational spectroscopy (NRVS), to determine the Fe vibrational density of states (VDOS).[1,2] NRVS has previously been applied to several heme compounds[3−6] and to the heme protein myoglobin,[7−9] providing vibrational spectra unconstrained by optical selection rules and specific to a single atom, i.e., Fe. We examine two very different monoheme proteins, myoglobin and cytochrome *f*, to observe the impact on Fe dynamics of Fe oxidation and spin state, and also the interactions between the heme and the amino acids of the protein backbone. The combination of NRVS with resonance Raman spectra allows the identification of those Raman active modes with significant Fe participation, which improves the assignment of mode characteristics to the Raman peaks. For this purpose we also measured resonant Raman spectra for cytochrome *f*, and are able to identify modes in Raman caused by Fe motions, and modes in NRVS not previously seen with Raman.

Heme proteins are often characterized by the electronic properties of the Fe atom, guided by the wealth of knowledge obtained from studies of model porphyrin compounds.[10] In deoxymyoglobin (DMb), the Fe has six d electrons in a high-spin ($S = 2$) configuration, bonded to the four planar porphyrin N atoms and to a His ligand in the fifth position. Metmyoglobin (metMb) has the same ligands, and in addition a water molecule bound in the sixth position, with five d electrons in a high-spin $S = {}^5/_2$ configuration. Cytochrome *f* has a unique sixth ligand, the *N*-terminus of the protein backbone,[11] which when oxidized has 5 d electrons in a low-spin ($S = {}^1/_2$) state, and when reduced has 6 d electrons in the $S = 0$ state (Table 1). From the point of view of the interaction between the heme molecule and the host protein, myoglobin is clearly in the weak-coupling limit, since the heme is bound to the protein only through the single Fe−His bond (Figure 1). There are no covalent attachments to any other part of the heme, which sits in a pocket where small

TABLE 1: Physical Properties of Fe in Myoglobin and Cytochrome *f* [a]

protein	deoxymyoglobin (DMb)	metmyoglobin (metMb)	cytochrome f, oxidized	cytochrome f, reduced
d-electron configuration	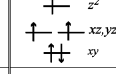	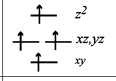	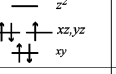	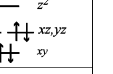
charge	d^6	d^5	d^5	d^6
spin	2	5/2	1/2	0
ligands	His-Fe	His-Fe-OH_2	His-Fe-Met & 2 heme-Cys	His-Fe-Met & 2 heme-Cys
mean force constant (N/m)	174 ±16	245 ±9	313 ±34	342 ±18
DOS at protein peak (30 cm^{-1})	60.1	48.3	21.6	29.7
DOS at 350 cm^{-1}	≤ 50	~90	164	165

[a] The d-electron configurations are shown schematically as occupying the atomic d levels of an isolated Fe atom, along with the standard charge and spin state assignments. The ligands describe the binding to the fifth and sixth Fe positions; the two heme−cysteine linkages for cytochrome *f* are also noted, to emphasize how the Fe atom is coupled to the protein. Mean force constants are deduced from the vibrational densities of states obtained by nuclear resonance vibrational spectroscopy; the error limits listed are due to statistical uncertainties only. DOS at protein peak tabulates the peak value of the Fe vibrational density of states near 30 cm^{-1} derived from the NRVS data, which is proportional to the frequency-weighted mean-squared Fe atomic displacement; the final column shows the same for the DOS peak near 350 cm^{-1}. Larger mean force constant correlates with larger displacements at high frequency, but smaller at the low-frequency protein peak.

* Address correspondence to this author: Phone: 765-494-6426. Fax: 765-494-0706. E-mail: durbin@physics.purdue.edu.
[⊥] Department of Physics, Purdue University.
[†] Department of Biological Sciences, Purdue University.
[‡] Argonne National Laboratory.
[§] Knox College.

10.1021/jp053440r CCC: $33.50
Published on Web 12/09/2005

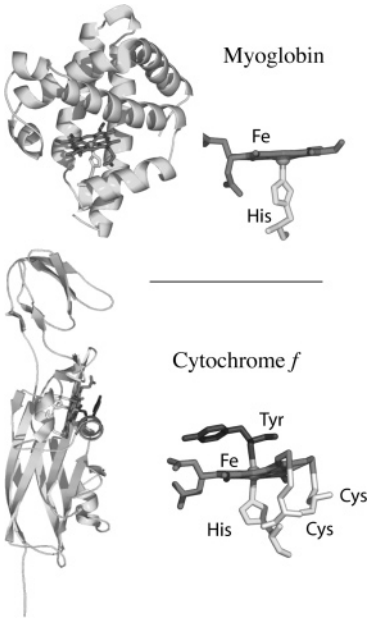

Figure 1. Ribbon diagrams and heme configurations for myoglobin and cytochrome *f*. Top: The heme molecule in myoglobin has a single bond between the Fe atom and a His residue of the protein backbone. Bottom: Cytochrome *f* has the same Fe−His bond, plus the two cysteine linckages characteristic of *c*-type cytochromes, and a unique Fe bond to the N terminus of the protein.

ligands such as O_2 can bind to the sixth Fe bond position. van der Waals interactions help stabilize the heme in the pocket. Cytochrome *f*, on the other hand, has two covalent heme−cysteine linkages characteristic of *c*-type cytochromes, plus the same Fe−His bond and the direct bond to the protein's *N*-terminus. These four covalent bonds put cytochrome *f* well into the strong-coupling limit.

II. Materials and Methods

NRVS is sensitive exclusively to the ^{57}Fe isotope, requiring enrichment of most samples. Protein preparation and measurement procedures are presented below.

A. Protein Preparation. Cytochrome *f* is the largest (ca. 286 amino acids, MW 31 864) of eight polypeptide subunits in the membrane-embedded cytochrome b_6f complex that functions in proton-coupled electron transfer and generation of the transmembrane electrochemical proton gradient.[12] A peptide segment approximately 35 residues long anchors cytochrome *f* to the membrane. High-resolution X-ray diffraction data have recently been obtained for the intact cytochrome b_6f complex;[13,14] the structure for isolated cytochrome *f* was determined previously.[11]

For the NRVS measurement, ^{57}Fe-enriched cytochrome *f* must be grown in sufficient quantities and converted to a ferrous state. NRVS utilizes the Mössbauer resonance of the ^{57}Fe nucleus, and over 10^{17} ^{57}Fe atoms are needed for practical measurement times. The natural abundance of ^{57}Fe is only 2.4%, however, making it difficult to get the minimum number of ^{57}Fe atoms into the appropriate sample volume. This required development of a method to introduce ^{57}Fe into the heme of cytochrome *f*. We achieved this by heterologous expression of the 251-residue extrinsic functional domain of cytochrome *f* in *Escherichia coli* grown in ^{57}Fe-enriched media. The pUCPF2 plasmid (cytochrome *f* expression construct[15]) was co-transformed with pEC86 that carries the cassette of cytochrome *c* maturation genes into strain XL1-Blue. The cells were grown semi-anaerobically at 37C for 20−24 h, harvested, and broken by osmotic shock through successive incubation first in sucrose buffer (20% sucrose, 30 mM Tris-HCl, pH 7.5, 1 mM EDTA) and then in distilled water. Crude cytochrome *f* in the supernatant was passed through a DE-52 ion-exchange column. Fractions containing cytochrome *f* were then pooled, concentrated, and passed through a Sephadex G-100 size-exclusion column. Cytochrome *f* fractions with A554/A280 > 0.7 were then passed through a hydroxyapatite column; fractions with A554/A280 > 0.9 were collected. The enrichment of ^{57}Fe in cytochrome *f* was achieved by growing the transformed E. coli cells in an optimized Fe-deficient liquid medium supplemented with 10 mM ^{57}Fe. The Fe-deficient liquid medium is made up of (g/L) casamino acids (8), yeast extract (1), glucose (1), $K_2HPO{\cdot}H_2O$ (3.4), KH_2PO_4 (5.7), NaCl (10), NH_4Cl (1.5), $MgSO_4$ (0.24), $CaCl_2$ (0.15), and KNO_3 (0.1), and adjusted with NaOH to pH 6.8−6.9. $^{57}Fe_2O_3$ was purchased from Cambridge Isotope Laboratories, Inc. and dissolved in HCl. The Fe content in the medium was measured by Inductively Coupled Plasma-Atomic Emission Spectroscopy (ICPAES). An enrichment of 80% ^{57}Fe was estimated by the content of Fe in the medium with and without the supplement of ^{57}Fe.

Purified cytochrome *f* in 10 mM Tris/HCl (pH 7.5) was reduced with ascorbate (ascorbate:cyt f = 5:1 (mol/mol)) and was monitored by absorption spectroscopy. The reduced cytochrome *f* was concentrated to 40 mg/mL with a Centricon, and then lyophilized. Fifteen milligrams of powdered cytochrome *f* was loaded into a sample cell ($4 \times 2 \times 8$ mm^3; 0.064 mL volume) and dissolved in water, resulting in a concentration of about 230 mg/mL.

For comparison purposes, we also prepared a smaller quantity of oxidized cytochrome *f*. The presence of Fe in the commonly used oxidant ferricyanide rules out its use here, since the specimen would contain excess Fe that would interfere with the heme Fe NRVS signal. We utilized instead Na_2IrCl_6 at a 10:1 molar ratio to cytochrome *f*, and confirmed the oxidation state with visible absorption spectroscopy.

The NRVS results are compared to similar data from deoxymyoglobin (DMb) and metmyoglobin (metMb). The DMb data and procedures were published previously.[7,16] The metMb preparation follows the work of Teale.[17] Starting material was lyophilized horse heart Mb (Sigma), from which the hemes were removed with methyl ethyl ketone. The apo-Mb was characterized by optical absorption as over 98% heme-free. Protoporphyrin-IX enriched to over 96% with ^{57}Fe, purchased from Frontier Scientific, Inc., was added to the apo-Mb. Uptake of the heme was monitored by Soret-band absorption. After concentration via Centricon YM-3 (Millipore) to 8 mM, samples were flash-frozen in liquid N_2. Both DMb and metMb were at pH 7.5 (100 mM Tris) before freezing.

B. Mössbauer. Mössbauer spectroscopy was employed to directly determine the concentration of ^{57}Fe nuclei in the enriched cytochrome *f*. Measurements were made on a constant acceleration spectrometer at 85 and 150 K in a 300 G field perpendicular to the γ-ray beam, where the total absorption area could be compared with that of a variety of 5- and 6-coordinate standard porphyrin model compounds. Assuming similar recoilless fractions for cytochrome *f* and the model compounds, we found that enrichment exceeding 70% was achieved, close to the 80% estimated from ICPAES.

C. Resonance Raman. Resonance Raman spectra were recorded at 10 K in the backscattering geometry. Samples were placed in a quartz couvette inside a variable-temperature, continuous-flow optical cryostat (Janis model SuperTran VP-100). The scattered radiation was excited with 413.1, 520.8, and 530.9 nm lines of a Kr^+ laser, the 528.7 nm line of an Ar^+

laser, and a 420.8 nm line from a Stilbene 3 dye laser, pumped by the Ar^+ laser. A cylindrical lens focused the incident laser radiation onto the sample with the laser beam of 0.2 by 5.0 mm^2 cross section, resulting in incident intensities of $\sim$1 W/cm^2. The scattered radiation was analyzed by a Spex-1401 double pass grating spectrometer and detected with a thermoelectrically cooled photomultiplier operating in the standard single-photon counting mode. Spectral resolution of the spectrometer was set to 4 cm^{-1}. The recorded spectra consisted of sharp Raman lines superposed on a broad fluorescence background. For the convenience of analysis the fluorescence was subtracted digitally.

D. NRVS. An X-ray can be resonantly absorbed by the ^{57}Fe nucleus when the X-ray energy E_x is within the exceedingly narrow Mössbauer line width (about 10^{-8} eV) of the resonance ($E_o \approx 14.413$ keV). If the difference between E_x and E_o matches the energy of a vibrational quantum of the system E_{vib}, however, absorption can occur, e.g., if $E_x + E_{vib} = E_o$. There are two critical properties of the X-ray beam that require a specialized beamline at a third generation X-ray synchrotron: there must be a sufficiently large number of X-ray photons within the 10^{-8} eV bandwidth to excite acceptable count rates, and this excitation beam must have an energy band-pass about E_x that is narrower than typical vibrational energies; about 1 meV (or 8 cm^{-1}) is desirable. Samples that contain nearly 10^{18} resonant Fe atoms will require data collection times of at least several hours, and sometimes much more.

Iron dynamics are probed by measuring the X-ray absorption spectrum over a typical energy range of 0$-$700 cm^{-1} about the resonance. By scanning the X-ray energy both below and above the resonance energy E_o, the Stokes (phonon creation) and anti-Stokes (phonon absorption) components of the absorption spectrum are obtained. This provides a direct measure of the sample temperature, and allows for the extraction of the Fe partial vibrational density of states, using the PHOENIX program.[3,18,19] The ability to convert NRVS data into quantitative parameters of Fe dynamics follows from application of Lipkin's sum rules[20] for the moments of the excitation energy spectrum:

$$\sum_f \frac{1}{\bar{\sigma}} \int \mathrm{d}E (E_f - E_i - R)^n \sigma_{i\rightarrow f}(E)$$

where E_i and E_f are the energies of the initial and final states, R is the free recoil energy of the nucleus, σ is the scattering cross section, and n is the order of the moment. A bar over a quantity, e.g., $\bar{\sigma}$, indicates integrating over all energies E and all final states f; hence, $\bar{\sigma}$ is the total integrated cross section for absorption by the nucleus. The scattered intensity measured in NRVS is essentially the cross section $\sigma_{i\rightarrow f}(E)$ convoluted with an instrumental resolution function, which can be accurately measured. Lipkin proved that the first moment is identically zero, which permits an absolute normalization of the measured scan since the value of R is a known quantity. The second moment is equal to $4R\bar{T}$, where $\bar{T}$ is the average kinetic energy of the absorbing nucleus (for isotropic samples), and the third moment is $R\hbar^2\overline{\omega^2}$, where ω values are the normal-mode frequencies; this yields the average force constant.

By assuming harmonic interactions between the Fe atom and its neighbors, the contribution from single vibrational modes can be separated from that of multiple excitations, and the Fe partial vibrational density of states (VDOS) determined. This approximation is only for convenience; theoretical refinements can be made to the data without the harmonic approximation.

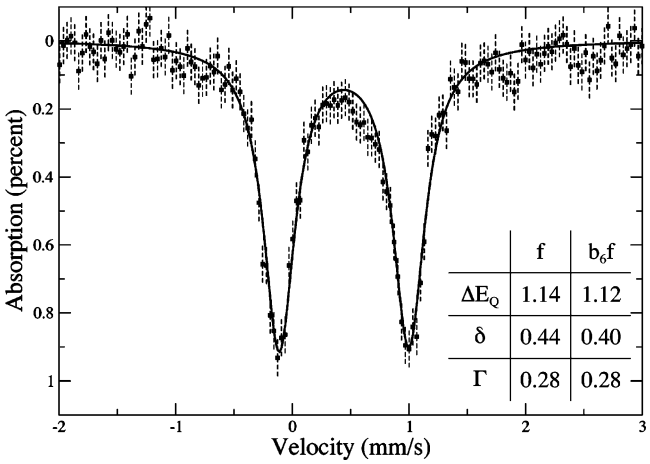

Figure 2. Mössbauer absorption spectrum for cytochrome *f* (reduced) at 150 K. The percent absorbed was converted to ^{57}Fe enrichment by comparing this scan to those of calibration specimens of heme model compounds. Inset: Electric quadrupole splitting (ΔE_Q), isomer shift (δ), and line width (Γ) are compared for this cytochrome *f* spectrum and the component of the cytochrome b_6f complex attributed to cytochrome *f* by Schünemann et al.,[25] confirming their assignment.

Further details of the NRVS technique and data analysis are described elsewhere.[16,21−24]

Measurements were conducted at the XOR-CAT sector 3-ID-D station of the Advanced Photon Source, Argonne National Laboratory. Specimens were placed in machined sapphire sample holders and cooled to about 20 K. The resonant absorption of the incident X-rays is monitored by Fe K fluorescence observed with a time-resolving Si avalanche photodiode detector. The instrumental resolution function was carefully measured by using the resonant forward-scattered Fe radiation of 7 cm^{-1}.

III. Results and Analysis

Mössbauer absorption spectroscopy was originally employed to simply measure the concentration of ^{57}Fe nuclei in the cytochrome *f* preparations. However, it also yields parameters such as the electric quadrupole splitting, ΔE_Q, and the isomer shift, δ, hyperfine properties that can be utilized to compare the Fe configuration in cytochrome *f* with that of related hemes and model compounds. Mössbauer absorption spectroscopy was previously reported on the entire cytochrome b_6f complex,[25] which contains one cytochrome *f*, one cytochrome *b*, and a 2Fe-2S Rieske iron$-$sulfur protein. (Recent X-ray crystallographic determination of the cytochrome b_6f structure at 3.0 Å resolution[13,14] has revealed a previously unknown and unique type of heme that might also contribute to the Mössbauer spectra of the entire complex.) Spectra from the cytochrome b_6f complex are separated into four separate Fe absorption patterns. On the basis of similarities with model hemes, the spectral shifts in the presence of magnetic fields, and the known chemical states of the Fe atoms, Schünemann et al.[25] assigned each of the four identifiable traces with the four known configurations of Fe. The measurements reported here (Figure 2) are the first Mössbauer spectra on isolated cytochrome *f*, and the data clearly support the earlier assignment of the cytochrome *f* spectrum: the values for the quadrupole splitting are nearly identical (1.14 vs 1.12 mm/s), as are the isomer shifts (0.44 vs 0.40). These slight differences can be accounted for by the temperature dependence of the second-order Doppler shift. These values are consistent with those observed for other low-spin, ferrous, six-coordinate model compounds.[26]

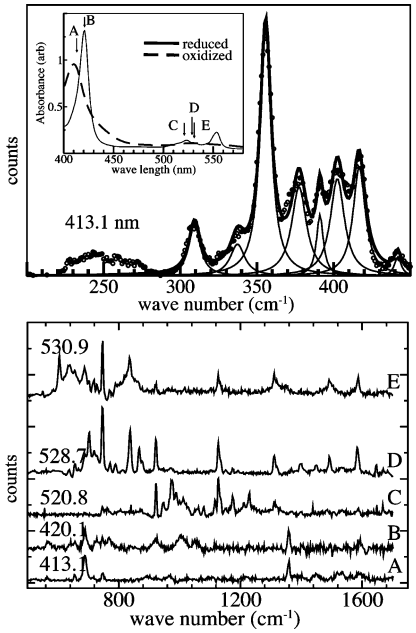

Figure 3. Raman spectroscopy on cytochrome *f* (reduced). Top, inset: Absorption spectra for cytochrome *f* (reduced and oxidized) showing the peaks relevant for resonance excitation. Labeled arrows denote wavelengths used for Raman measurements: A, 413.1 nm; B, 420.1 nm; C, 520.8 nm; D, 528.7 nm; and E, 530.9 nm. Top: Raman spectrum at 413.1 nm (circles), results of peak fitting from 280 to 450 cm^{-1}, using Voigt trial functions (thin lines), and the total best fit curve (thick line). Bottom: Raman spectra for all five wavelengths for 450−1700 cm^{-1}; the variability of peak heights with wavelength illustrates the difficulty of assessing amplitudes of vibrational modes from resonant Raman spectra.

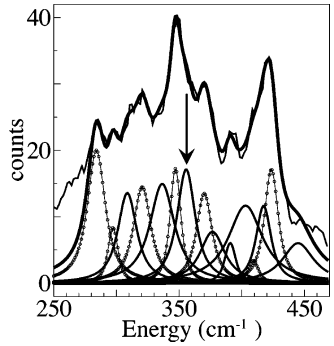

Figure 4. NRVS spectrum and peak fitting for cytochrome *f*. The NRVS scattered intensity for cytochrome *f* (reduced) is represented by a thin black line for the same spectral region used for Raman peak fitting (Figure 3). The arrow denotes the most intense "ν_8" line in the Raman spectrum, at 356 cm^{-1}. The same peak-fitting algorithm applied to these data started with the eight Raman lines (shown here as solid black lines), and required seven additional peaks (lines with circle symbols) to produce the fit to the data shown as the heavy black line. These extra peaks correspond to previously unseen modes with significant Fe motion that are not Raman allowed.

Cytochrome *f* was first studied with resonance Raman scattering by Davis et al.,[27] which revealed structure in the high frequency regime, and more recently by Gao et al.[28] using Q-band resonance and by Picaud et al.[29] on the cytochrome b_6f complex. Their results overall are consistent with the spectra reported here, considering the differences in excitation wavelength, for example. Our resonance Raman studies of cytochrome *f* were conducted at five different wavelengths near features in the absorption spectrum, and as seen in Figure 3 the amplitudes of all peaks change significantly and unpredictably from one wavelength to the next. This is a fundamental characteristic of resonance Raman: the peak height depends both on the amplitude of vibration and on an unknown coupling strength between the vibration and the resonantly excited electronic state. Raman spectra accurately determine the energies of vibrational modes, but the amplitudes are only qualitative at best. These spectra are also confined to Raman-active modes, which can be a significant limitation for molecules of high symmetry.

Figure 3 includes a detailed scan at 413.1 nm highlighting a region below ∼500 cm^{-1}, where most contributions from the heavy Fe atom are expected. Standard peak-fitting routines based on Voigt functions (convolutions of a Lorentzian with a Gaussian) were employed to identify 8 separate peaks in the cluster between 300 and 450 cm^{-1}, where an attempt was made to keep the number of trial peaks to a minimum. Table 1 includes the best-fit peak positions and peak widths, after accounting for the 4 cm^{-1} resolution of the Raman data.

The largest peak at 356 cm^{-1} corresponds to ν_8, based on long-established convention. Abe et al.[30] in 1978 provided this label for a particular mode (observed at 344 cm^{-1}) of A_{1g} symmetry in a normal coordinate analysis of resonant Raman data on Ni(II) octaethylporphyrin (NiOEP). A similar combined resonance Raman-normal-mode analysis of Ni(II) porphine (NiP) and Ni(II) tetraphenlyporphyrin (NiTPP) in 1990 assigned the ν_8 mode to lines at 369 and 402 cm^{-1}, respectively.[31] The same type of analysis was extended in 1993 to the protein, cytochrome *c*, using isotopic substitutions, and assigned the ν_8 mode to a Raman peak at 347 cm^{-1}.[32] As one further example, the ν_8 was assigned to a peak near 344 cm^{-1} in a study of microperoxidases, which in this case were fragments of the cytochrome *c* protein that include only 8 protein residues.[33]

NRVS data for the same spectral region in cytochrome *f* are displayed in Figure 4, with the results of the same peak-fitting protocol previously applied to the Raman data. One sees immediately that NRVS reveals more modes than the Raman scan, a result of its intrinsic sensitivity to all modes with significant Fe amplitudes. The fitting was done by first assuming trial peaks with the same energy and widths as the eight peaks seen by Raman (Figure 3), but allowing the amplitude to vary. Physically this corresponds to assuming that each of the Raman-active modes includes motion of the Fe atom. It proved necessary, however, to add seven additional peaks to obtain a good fit (see Table 2).

This comparison of the Raman and NRVS spectra demonstrates the advantage of not being constrained by optical selection rules. Furthermore, it provides a strong case that much if not all of the Raman intensity in this region must come from modes with significant Fe participation, because each of the Raman peaks overlaps regions of NRVS intensity. It is interesting to consider the case of the ν_8 mode, indicated by the arrow in Figure 4 at 356 cm^{-1}. If this does in fact correspond to a mode in the NRVS data, then it must have a large Fe displacement. The symmetry of this mode in the bare porphyrin molecule, however, requires there be no Fe motion at all.[32] When put into the protein as protoporphyrin IX, the symmetry requirement may be relaxed due to structural modifications. In that case, however, the mode will have lost its ν_8 character, and this label then has little meaning.

We also consider the possibility that the Raman peak at 356 cm^{-1} really has ν_8 character with negligible Fe motion, but it is not possible to fit these data without a peak near 356 cm^{-1}. There cannot be two modes with different Fe displacements at the same frequency; it seems unlikely that a prominent Raman mode with no Fe displacement is found in this energy region.

TABLE 2: Peak-Fitting Results for the 280−450 cm^{-1} NRVS Spectrum[a]

	NRVS position (cm^{-1})	Raman	intrinsic width (cm^{-1})
1	284		2.6
2	297		1.2
3	309	√	2.8
4	320		2.5
5	336	√	3.4
6	347		1.3
7	356	√	2.7
8	370		2.2
9	377	√	3.8
10	391	√	1.3
11	403	√	5.4
12	409		1.2
13	417	√	2.1
14	423		1.9
15	445	√	4.9

[a] Fifteen peaks were obtained from the cytochrome *f* NRVS data (Figure 4), using the same procedure employed for the Raman spectrum (Figure 3). The fitting assumed a Voigt peak shape whose Gaussian fwhm of 7 cm^{-1} (from the measured instrumental resolution function) was convoluted with a Lorentzian "intrinsic" width. Listed are the central peak energy and intrinsic widths. The eight peaks listed as "√" for Raman have the same positions and widths found from the same procedure applied to the Raman data; the fit to NRVS requires seven additional peaks.

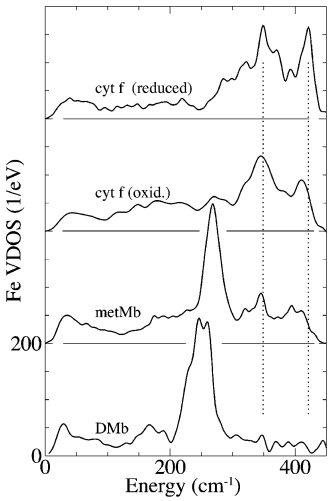

Figure 5. Fe vibrational density of states for oxidized and reduced cytochrome *f*, metmyoglobin, and deoxy-myoglobin. Vibrational densities of states (VDOS) obtained from NRVS data with the PHOENIX program[19] are shown (displaced vertically for clarity) for these four monoheme proteins, whose binding characteristics, charge and spin states, and average force constants are given in Table 1. The DMb VDOS has significant overlap with metMb, but little with cytochrome *f*. The two dotted vertical lines are a guide to the eye. (VDOS for DMb are derived from data published in Sage et al. (2001).[7])

The NRVS scattering data for cytochrome *f* have been converted to Fe vibrational density of states (VDOS),[19] and compared to similar spectra for deoxymyoglobin (DMb), which has nothing bonded to the sixth Fe position, and metmyoglobin (metMb), where Fe binds a water molecule (Figure 5). Because of the internal normalization of NRVS data described by the Lipkin sum rules, these VDOS spectra are known on an absolute scale, equivalent to describing the absolute magnitude of Fe atom amplitudes as a function of frequency. These spectra therefore provide a stringent validity test for any calculation of myoglobin or cytochrome *f* normal modes, as can be routinely done by the major molecular dynamics computational packages (e.g., CHARMM[34,35]).

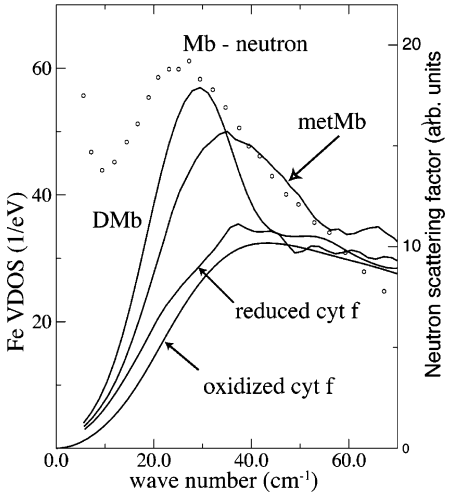

Figure 6. Fe vibrational densities of state from Figure 5 compared with inelastic neutron scattering measurement of the protein scattering factor in the protein peak region. Solid curves are for DMb, metMb, and reduced and oxidized cytochrome *f*. Circles are scattering factors obtained from inelastic neutron spectroscopy on metMb published by Cusack and Doster,[37] primarily due to protein backbone vibrations via scattering from H atoms. The overlap between the protein scattering from the neutrons and the Fe scattering in NRVS shows that the heme participates in protein modes; the relative suppression for cytochrome *f* correlates with the strong-binding configuration of its heme.

Examination of these VDOS spectra shows that when DMb is converted to metMb by binding a water molecule to the Fe atom, there is a slight hardening of the main feature near 250 cm^{-1} (associated largely with in-plane modes[7]), and some increase in modes at higher frequencies. This hardening in metMb is also associated with a reduction of Fe−N bond lengths, and a shift in position of the Fe atom from about 0.3 Å below the heme plane to being nearly coplanar with the heme.[36] With cytochrome *f*, however, nearly all of the VDOS occurs at higher frequencies, meaning that the Fe atom is constrained by much stronger forces in cytochrome *f* than in myoglobin.

The charge and spin states corresponding to the expected d electron distributions in deoxymyoglobin, metmyoglobin, and cytochrome *f* in the reduced and oxidized states are illustrated in Table 1, as well as the progression of ligands and the mean force constants derived from the VDOS. Several trends are apparent: the force constant is significantly larger for cytochrome *f* than myoglobin, it increases with decreasing spin, and is also correlated with the ligand configuration. Spin plays no explicit role in the force on Fe, but it can be an indicator of the nature of the orbitals that determine the strength of the interaction with neighboring atoms. It is not immediately obvious how the charge and spin of the atomic orbitals would produce the observed pattern of force constants, suggesting that ab initio calculations of the heme group may be needed to shed light on this aspect of the Fe potential.

It is important to note that the coupling of the heme to the protein is likely to influence Fe dynamics beyond what can be inferred from the heme group alone. Figure 6 replots the low-frequency VDOS feature near 25−30 cm^{-1}, the "protein peak" representing the spectral range where the normal modes of the protein backbone have their largest amplitudes. These dynamics are seen directly with inelastic neutron scattering; a previous measurement of the neutron dynamical structure factor for myoglobin is also plotted in Figure 5.[37] Those authors concluded that the "dominant...displacements occur in myoglobin with a frequency of 25 cm^{-1}." A comparison with the NRVS results

finds that DMb has the largest heme Fe amplitude at the same peak frequency, metMb is somewhat reduced and shifted toward slightly higher frequencies, and the phenomenon is almost completely suppressed in cytochrome *f*. The behavior of the protein peak as reflected in the Fe VDOS demonstrates the importance of including the protein when considering Fe dynamics in these heme proteins.

This VDOS does depend explicitly on the Fe vibrational amplitudes appropriately weighted over all normal modes of the system. (See eqs 4−6 in ref 3.) We can approximate this relationship by observing that the VDOS is proportional to the square of the Fe amplitudes multiplied by the energy. Table 1 includes the DOS values for DMb, metMb, cyt *f* (oxidized), and cyt *f* (reduced) both at the protein peak near 30 cm^{-1} and near the largest feature at 350 cm^{-1}. One sees that the protein peak VDOS, and therefore the Fe vibrational amplitudes, is much smaller in the cytochromes than in Mb, opposite the trend in mean force constants. On the other hand, the Fe amplitudes are much larger in the cytochromes at the higher frequency (350 cm^{-1}).

The trends shown in Figure 6, as well as the force constants in Table 1, suggest that the cytochrome heme must be more rigidly entrained by the protein, with significantly reduced Fe displacements despite the more direct coupling to the vibrational modes of the protein. (Similar conclusions have been drawn from a laboratory-based Mössbauer study of cytochrome *c* that examined the temperature dependence of the Fe mean displacements derived from Lamb−Mössbauer factors.[38,39]) The more flexible Fe configuration in Mb (and hemoglobin (Hb)) may be critical for binding to small molecules, as well as for the change in protein conformation comprising the allosteric response to binding in Mb and Hb. A functional benefit from heme stiffness in electron-transfer cytochromes is not yet evident. Further studies will be required to confirm a correlation between the nature of heme−protein dynamical coupling and biochemical function.

An underlying assumption in this analysis is that if a peak appears with the same energy with use of two different vibrational spectroscopies, such as Raman and NRVS, then in general the two techniques are measuring the same normal mode. In a set of coupled oscillators such as a protein molecule, two distinct normal modes cannot have the same energy, since the excitation of one mode would resonantly excite the second mode in a coherent manner, which simply means they would then be the same normal mode. In the case of inelastic neutron scattering, the protein peak appears as a continuum of modes due to the high mode density that results from the large number of atoms in the protein. These modes can also overlap due to instrumental, lifetime, or inhomogeneous broadening from various types of conformational disorder. Neutrons are scattered almost entirely by the hydrogen atoms of the protein backbone, and hence are largely insensitive to the heme molecule. NRVS, on the other hand, only sees the Fe atom in the heme molecule. Since the protein peak is clearly manifested in both spectroscopies, they both are sensing the same normal modes. This is a clear experimental demonstration that in this frequency range the heme molecule is coherently moving with the protein. There cannot be separate heme modes and protein modes; instead, the normal modes are composed of both. The nature of these collective modes is central to the mechanism for energy transport in proteins: conformational changes induced by ligand binding, photoabsorption, or electron transfer must propagate from the reaction center to the entire protein via a superposition of normal modes.[40−44]

IV. Conclusions

The Fe vibrational density of states for myoglobin and cytochrome *f*, measured with nuclear resonance vibrational spectroscopy, provides a detailed description of heme dynamics that complements resonance Raman and inelastic neutron spectroscopies. The VDOS and deduced average force constants can be compared with charge and spin states as well as with specific structural configurations. More importantly, the low-frequency spectral regions reveal the explicit coupling of Fe to the protein, which is likely to be critical for probing how protein dynamics influence the function of the heme reaction center. These VDOS are amenable to comparison with empirical potential molecular dynamics simulations, providing an experimental check on predicted Fe normal modes for the four monoheme proteins examined here. The question of a correlation between heme dynamics and biological function should be an interesting future direction for this spectroscopy.

Acknowledgment. We acknowledge S. Heimann for important contributions in early stages of this study, Chenfeng Zhang for data collection at the synchrotron, and E. W. Prohofsky for valuable discussions. This work was supported by the National Science Foundation through Award No. PHY-9988763, the IDHM Program of the Center for Sensing Science and Technology, Purdue University, and NSWC Crane Contract No. N00164-00-C-0047. Use of the Advanced Photon Source was supported by the U.S. Department of Energy, Basic Energy Sciences, Office of Science, under Contract No. W-31-109-Eng-38.

References and Notes

(1) Scheidt, W. R.; Durbin, S. M.; Sage, J. T. *J. Inorg. Biochem.* **2005**, *99*, 60.

(2) Sturhahn, W. *J. Phys.-Condens. Matter* **2004**, *16*, S497.

(3) Rai, B. K.; Durbin, S. M.; Prohofsky, E. W.; Sage, J. T.; Wyllie, G. R. A.; Scheidt, W. R.; Sturhahn, W.; Alp, E. E. *Biophys. J.* **2002**, *82*, 2951.

(4) Rai, B. K.; Durbin, S. M.; Prohofsky, E. W.; Sage, J. T.; Ellison, M. K.; Roth, A.; Scheidt, W. R.; Sturhahn, W.; Alp, E. E. *J. Am. Chem. Soc.* **2003**, *125*, 6927.

(5) Budarz, T. E.; Prohofsky, E. W.; Durbin, S. M.; Sjodin, T.; Sage, J. T.; Sturhahn, W.; Alp, E. E. *J. Phys. Chem. B* **2003**, *107*, 11170.

(6) Rai, B. K.; Durbin, S. M.; Prohofsky, E. W.; Sage, J. T.; Ellison, M. K.; Scheidt, W. R.; Sturhahn, W.; Alp, E. E. *Phys. Rev. E* **2002**, *66*.

(7) Sage, J. T.; Durbin, S. M.; Sturhahn, W.; Wharton, D. C.; Champion, P. M.; Hession, P.; Sutter, J.; Alp, E. E. *Phys. Rev. Lett.* **2001**, *86*, 4966.

(8) Achterhold, K.; Sturhahn, W.; Alp, E. E.; Parak, F. G. *Hyperfine Interact.* **2002**, *141*, 3.

(9) Achterhold, K.; Keppler, C.; Ostermann, A.; van Burck, U.; Sturhahn, W.; Alp, E. E.; Parak, F. G. *Phys. Rev. E* **2002**, *65*.

(10) Scheidt, W. R.; Reed, C. A. *Chem. Rev.* **1981**, *81*, 543.

(11) Carrell, C. J.; Schlarb, B. G.; Bendall, D. S.; Howe, C. J.; Cramer, W. A.; Smith, J. L. *Biochemistry* **1999**, *38*, 9590.

(12) Cramer, W. A.; Soriano, G. M.; Ponomarev, M.; Huang, D.; Zhang, H.; Martinez, S. E.; Smith, J. L. *Annu. Rev. Plant Physiol. Plant Mol. Biol.* **1996**, *47*, 477.

(13) Kurisu, G.; Zhang, H. M.; Smith, J. L.; Cramer, W. A. *Plant Cell Physiol.* **2004**, *45*, S44.

(14) Kurisu, G.; Zhang, H. M.; Smith, J. L.; Cramer, W. A. *Science* **2003**, *302*, 1009.

(15) Ponamarev, M. V.; Cramer, W. A. *Biochemistry* **1998**, *37*, 17199.

(16) Sage, J. T.; Paxson, C.; Wyllie, G. R. A.; Sturhahn, W.; Durbin, S. M.; Champion, P. M.; Alp, E. E.; Scheidt, W. R. *J. Phys.-Condens. Matter* **2001**, *13*, 7707.

(17) Teale, F. W. J. *Biochim. Biophys. Acta* **1959**, *35*, 543.

(18) Sturhahn, W.; Kohn, V. G. *Hyperfine Interact.* **1999**, *123*, 367.

(19) Sturhahn, W. *Hyperfine Interact.* **2000**, *125*, 149.

(20) Lipkin, H. J. *Phys. Rev. B* **1995**, *52*, 10073.

(21) Seto, M.; Yoda, Y.; Kikuta, S.; Zhang, X. W.; Ando, M. *Phys. Rev. Lett.* **1995**, *74*, 3828.

(22) Sturhahn, W.; Toellner, T. S.; Alp, E. E.; Zhang, X.; Ando, M.; Yoda, Y.; Kikuta, S.; Seto, M.; Kimball, C. W.; Dabrowski, B. *Phys. Rev. Lett.* **1995**, *74*, 3832.

(23) Keppler, C.; Achterhold, K.; Ostermann, A.; vanBurck, U.; Potzel, W.; Chumakov, A. I.; Baron, A. Q. R.; Ruffer, R.; Parak, F. *Eur. Biophys. J. Biophys. Lett.* **1997**, *25*, 221.

(24) Chumakov, A. I.; Sturhahn, W. *Hyperfine Interact.* **1999**, *123*, 781.

(25) Schunemann, V.; Trautwein, A. X.; Illerhaus, J.; Haehnel, W. *Biochemistry* **1999**, *38*, 8981.

(26) Debrunner, P. G. In *Iron Porphyrins − Part 3*; Lever, A. B. P., Gray, H. B., Eds.; VCH Publishers: New York, 1989; Chapter 2.

(27) Davis, D. J.; Frame, M. K.; Johnson, D. A. *Biochim. Biophys. Acta* **1988**, *936*, 61.

(28) Gao, F.; Qin, H.; Knaff, D. B.; Zhang, L.; Yu, L.; Yu, C. A.; Gray, K. A.; Daldal, F.; Ondrias, M. R. *Biochim. Biophys. Acta-Protein Struct. Mol. Enzymol.* **1999**, *1430*, 203.

(29) Picaud, T.; Le Moigne, C.; de Gracia, A. G.; Desbois, A. *Biochemistry* **2001**, *40*, 7309.

(30) Abe, M.; Kitagawa, T.; Kyogoku, Y. *J. Chem. Phys.* **1978**, *69*, 4526.

(31) Li, X. Y.; Czernuszewicz, R. S.; Kincaid, J. R.; Su, Y. O.; Spiro, T. G. *J. Phys. Chem.* **1990**, *94*, 31.

(32) Hu, S. Z.; Morris, I. K.; Singh, J. P.; Smith, K. M.; Spiro, T. G. *J. Am. Chem. Soc.* **1993**, *115*, 12446.

(33) Othman, S.; Lelirzin, A.; Desbois, A. *Biochemistry* **1994**, *33*, 15437.

(34) MacKerell, A. D.; Bashford, D.; Bellott, M.; Dunbrack, R. L.; Evanseck, J. D.; Field, M. J.; Fischer, S.; Gao, J.; Guo, H.; Ha, S.; Joseph-McCarthy, D.; Kuchnir, L.; Kuczera, K.; Lau, F. T. K.; Mattos, C.; Michnick, S.; Ngo, T.; Nguyen, D. T.; Prodhom, B.; Reiher, W. E.; Roux, B.; Schlenkrich, M.; Smith, J. C.; Stote, R.; Straub, J.; Watanabe, M.; Wiorkiewicz-Kuczera, J.; Yin, D.; Karplus, M. *J. Phys. Chem. B* **1998**, *102*, 3586.

(35) Melchers, B.; Knapp, E. W.; Parak, F.; Cordone, L.; Cupane, A.; Leone, M. *Biophys. J.* **1996**, *70*, 2092.

(36) Kachalova, G. S.; Popov, A. N.; Bartunik, H. D. *Science* **1999**, *284*, 473.

(37) Cusack, S.; Doster, W. *Biophys. J.* **1990**, *58*, 243.

(38) Frolov, E. N.; Gvosdev, R.; Goldanskii, V. I.; Parak, F. G. *J. Biol. Inorg. Chem.* **1997**, *2*, 710.

(39) Parak, F. G. *Curr. Opinion Struct. Biol.* **2003**, *13*, 552.

(40) Armstrong, M. R.; Ogilvie, J. P.; Cowan, M. L.; Nagy, A. M.; Miller, R. J. D. *Proc. Natl. Acad. Sci. U.S.A.* **2003**, *100*, 4990.

(41) Miller, R. J. D. *Can. J. Chem.-Rev. Can. Chim.* **2002**, *80*, 1.

(42) Xie, A. H.; van der Meer, A. F. G.; Austin, R. H. *Phys. Rev. Lett.* **2002**, *88*.

(43) Frauenfelder, H.; McMahon, B. H.; Fenimore, P. W. *Proc. Natl. Acad. Sci. U.S.A.* **2003**, *100*, 8615.

(44) Ansari, A.; Berendzen, J.; Bowne, S. F.; Frauenfelder, H.; Iben, I. E. T.; Sauke, T. B.; Shyamsunder, E.; Young, R. D. *Proc. Natl. Acad. Sci. U.S.A.* **1985**, *82*, 5000.